State-to-state modeling of a recombining nitrogen plasma experiment

C. Laux, Laurent Pierrot, Richard J. Gessman

Accepté pour publication, Chemical Physics, Oct. 2011

State-to-state modeling of a recombining nitrogen plasma experiment

Christophe O. Laux,[1,2,3] Laurent Pierrot,[3] Richard J. Gessman[3]

[1]Laboratoire EM2C, CNRS UPR288, Grande Voie des Vignes, 92290 Châtenay-Malabry, France

[2]Ecole Centrale Paris, Grande Voie des Vignes, 92290 Châtenay-Malabry, France

[3]Mechanical Engineering Department, Stanford University, Stanford CA 94305, USA

Abstract

An atmospheric pressure nitrogen/argon plasma flows at high velocity through a water-cooled test-section in which it is forced to recombine within 250 μs. At the test-section inlet, the plasma is in Local Thermodynamic Equilibrium (LTE) at about 7200 K. Because recombination rates are finite, the plasma reaches a state of chemical nonequilibrium at the exit of the test-section, at a temperature of about 4715 K. At the test-section exit, the radiation emitted by the plasma, measured by emission spectroscopy, shows significant departures from equilibrium in the populations of the excited electronic states of nitrogen (N_2 $B^3\Pi_g$, N_2 $C^3\Pi_u$) and of the nitrogen ion (N_2^+ $B^2\Sigma_u^+$). This experiment is thus proposed as a test-case to validate collisional-radiative (CR) models. A vibrationally specific CR model is then used to predict the emission of these states. The rate coefficients of the model are calculated with the Weighted Rate Coefficient method based on elementary cross-section data. These rates depend explicitly on the kinetic temperatures of electrons (T_e) and heavy species (T_g). The predictions of the CR model are in good agreement with the measured vibrational population distribution in the N_2 B state. A method is then proposed to determine ground state nitrogen atom densities based on the measured vibrational population distribution of the N_2 B state.

Introduction

The chemistry of nonequilibrium molecular plasmas is important to predict nonequilibrium radiation in atmospheric re-entry and to interpret optical diagnostics in applications ranging from material processing or biodecontamination to plasma-assisted combution. Simulating the radiation of recombining plasmas or reentry flows requires to predict the populations of the emitting internal levels of atoms and molecules under nonequilibrium conditions. Various forms of nonequilibrium can exist. We distinguish thermal nonequilibrium, where the kinetic temperature T_g of heavy species is different from the kinetic temperature T_e of the electrons, and chemical nonequilibrium, where chemical reactions are not equilibrated. Local Thermodynamic Equilibrium (LTE) corresponds to the case of both thermal and chemical equilibrium.

The nonequilibrium populations of internal energy states can be determined by solving the so-called master equation, which is a system of coupled state-specific rate equations (collisional-radiative model, or CR). While for atomic species it is usually sufficient to consider 10-100 electronic states, for molecular species a much larger number of rovibronic levels must be taken into account. Many CR models [1-5] use the simplifying assumption that the rotational and vibrational energy levels of molecules are populated according to Boltzmann distributions at temperatures T_r and T_v, respectively. In these models, the master equation is solved for electronic levels only, with global rates corresponding to averages over the rovibrational states of each electronic level. Thus these approaches implicitly assume that departures from Boltzmann distributions in the populations of rotational and vibrational levels are small.

Yet, departures from Boltzmann distributions, at least in the vibrational levels, are fairly common. Experiments conducted at Stanford University [6] with a nitrogen/argon plasma forced to recombine within 250 μs from a state of equilibrium at a temperature of 7200 K to a state of chemical nonequilibrium at 4715 K have shown that the populations of vibrational levels in certain electronic states, in particular the $B^3\Pi_g$ of N_2, can strongly depart from a Boltzmann distribution when the density of atomic nitrogen is higher than its LTE value. To predict nonequilibrium populations, a vibrational state-specific collisional-radiative (CR) model must be used. Most existing vibrational state-specific CR models [7-9] usually assume that the rotational levels follow a Boltzmann distribution owing to fast rotational relaxation, especially at atmospheric pressure. This assumption is also made in the present work.

In this paper, we first give an overview of the vibrational state-to-state CR model that we have developed for nitrogen plasmas [10-12]. The second part of the paper presents the recombining nitrogen plasma experiment [6] which is proposed as a test-case to validate nitrogen CR models. The third part compares the vibrational population distributions measured in that experiment with the simulations obtained with the nitrogen CR model. In the last part of the paper, we propose a method to determine absolute ground state N atom densities from the measured nonequilibrium emission of the N_2 B state.

1. Nitrogen CR model

Details about the nitrogen CR model and derivation of the vibrational state-specific rate coefficients are given by Pierrot et al. [10-12]. This model was subsequently extended to air plasmas [13], but these extensions will not presented because the focus of the present paper is on modeling a recombining nitrogen plasma. We give below an overview of the nitrogen CR model and of its capabilities.

Species and energy levels considered

The species considered in the nitrogen CR model are N, N^+, N_2, N_2^+, and electrons. The internal structure of N is accounted for by using the 22 grouped electronic levels of Park [14].

For N^+, only the ground state is taken into account. The X, A, B, W, B′, and C electronic states of N_2 and the X, A, and B electronic states of N_2^+ are included, and all rovibrational levels belonging to these states are considered up to the dissociation limit. As listed in [Insert Table 1, the model takes into account 192 vibronic levels of N_2 and 142 levels of N_2^+. Note that the model for the ground state of N_2 contains fewer vibrational levels that the more accurate model recently proposed by Le Roy *et al* [15] (48 levels for present model vs. 61 levels for Le Roy *et al*), but this difference has little impact on the excited state populations presented here.

[Insert Table 1.]

Reactions considered

The nitrogen CR model considers approximately 46,000 reactions that are summarized in [insert Table 2. These reactions include electron-impact ionization, excitation, and dissociation of atoms and molecules, heavy-particle impact dissociation of molecules, as well as electron-impact vibrational excitation of ground state nitrogen (VE transfer), vibrational-translational (VT) and vibrational-vibrational (VV) transfer, charge exchange, dissociative recombination, radiation, and predissociation.

[insert Table 2]

Example of rate coefficient calculation: N_2 ground state ionization by electron impact

To illustrate the principles of the vibrationally specific CR model, we present the method of calculation of the rate coefficients for electron-impact ionization of ground state N_2. We begin by considering the elementary ionization reaction between rovibronic level (X,v",J") of N_2 to level (A,v',J') of N_2^+.

$$N_2\,(X,v",J") + e \rightarrow N_2^+\,(A,v',J') + e + e$$

We first determine the rate coefficient of this elementary reaction, and then we average the elementary rate coefficients over all initial (J") and final (J') rotational levels of (X,v") and (A,v') in order to obtain the vibrational state-specific rate coefficients.

Elementary rate coefficients

The elementary rate coefficient of electron-impact ionization of N_2 (X,v",J") into N_2^+ (A,v',J'), can be written as:

$$K_{N_2Xv"J"}^{N_2^+Av'J'}(T_e) = \frac{8\pi}{\sqrt{m_e}} \frac{1}{(2\pi k T_e)^{3/2}} \int_0^{+\infty} \varepsilon \sigma_{N_2Xv"J"}^{N_2^+Av'J'}(\varepsilon) \exp\left(-\frac{\varepsilon}{kT_e}\right) d\varepsilon \qquad (1)$$

where $\sigma_{N_2Xv"J"}^{N_2^+Av'J'}(\varepsilon)$ is the cross-section of the elementary reaction, m_e the electron mass, and ε the electron energy. In Eqn. (1), we have implicitly assumed that electrons follow a Maxwellian energy distribution at temperature T_e. In passing, we note that all rate coefficients of the CR

model assume Maxwellian energy distributions for electrons and heavy species at T_e and T_g, respectively. Although this assumption is not justified in general for electrons, we will see later that it is valid for the conditions of the recombination experiment presented in this paper.

Following Park [14], we consider that the Franck-Condon principle holds for transitions in molecules caused by collisions with electrons, and that no change in rotational quantum number occurs as a result of such collisions. Accordingly, we write the elementary cross-section of ionization from rovibronic level N_2 (X,v",J") to rovibronic level N_2^+ (A',v',J') as:

$$\sigma_{\mathrm{N_2Xv"J"}}^{\mathrm{N_2^+Av'J'}} = q_{\mathrm{Xv"}}^{\mathrm{Av'}}\ \delta_J^{J'}\,\chi\left(\varepsilon, \Delta E_{\mathrm{Xv'J'}}^{\mathrm{Av'J'}}\right) \tag{2}$$

where $q_{\mathrm{Xv"}}^{\mathrm{Av'}}$ designates the Franck-Condon factor, $\Delta E_{\mathrm{Xv"J"}}^{\mathrm{Av'J'}}$ the ionization energy, and $\delta_{J"}^{J'}$ is equal to 1 if J" = J' and to 0 otherwise. The reduced cross-section $\chi(\varepsilon, \Delta E_{\mathrm{Xv"J"}}^{\mathrm{Av'J'}})$ is calculated with the Binary-Encounter-Bethe (BEB) model of Hwang *et al* [17], which provides ionization cross-sections within 15% of experimental values for a wide variety of atoms and molecules. The BEB expression is:

$$\chi\left(\varepsilon, \Delta E_{\mathrm{Xv'J'}}^{\mathrm{Av'J'}}\right) = 4\pi a_0^2 N \left(\frac{R}{\Delta E_{\mathrm{Xv'J'}}^{\mathrm{Av'J'}}}\right)^2 \frac{1}{t+u+1}\left[\frac{\ln t}{2}\left(1-\frac{1}{t^2}\right)+1-\frac{1}{t}-\frac{\ln t}{t+1}\right] \tag{3}$$

where R is the Rydberg constant (13.61 eV), a_0 is the Bohr radius (0.5292 Å), N is the electron occupation number in the shell from which ionization takes place, t stands for $\varepsilon/\Delta E_{\mathrm{Xv"J"}}^{\mathrm{Av'J'}}$ where ε is the kinetic energy of the electron, and u stands for $\mathrm{U}/\Delta E_{\mathrm{Xv"J"}}^{\mathrm{Av'J'}}$ where U is the average kinetic energy of a bound electron in the shell. The values of N and U are given by Hwang *et al* [17] for several molecular orbitals of N_2 and O_2.

Vibrational state-specific rate coefficients

To obtain the vibrational state-specific rate coefficients, we sum the elementary rate coefficients over all final rotational levels, and we average over the distribution of initial rotational levels. We assume that the initial rotational levels follow a Boltzmann distribution at rotational temperature T_r, which is a reasonable approximation for many molecules of interest (except perhaps the hydrides) owing to fast collisional relaxation at atmospheric pressure. The vibrational state specific rate coefficient is then:

$$K_{\mathrm{N_2Xv"}}^{\mathrm{N_2^+Av'}}\left(T_e, T_r\right) = \frac{1}{Q_{\mathrm{rot}}^{\mathrm{N_2Xv"}}\left(T_r\right)} \times \sum_{J"}\left(2J"+1\right)\exp\left[-\frac{F_{\mathrm{N_2Xv"}}\left(J"\right)}{kT_r}\right]\sum_{\mathrm{J'}} K_{\mathrm{N_2Xv"J"}}^{\mathrm{N_2^+Av'J'}}\left(T_e\right) \tag{4}$$

where $Q_{\mathrm{rot}}^{N_2,X,\mathrm{v"}}$ is the rotational partition function of N_2 in level X,v", and $F_{\mathrm{N_2Xv"}}\left(J"\right)$ is the rotational term energy of level J". The reverse rates are determined by detailed balance.

We compare in [insert Table 3 the total vibrationally specific ionization cross-sections of $N_2(X^1\Sigma_g^+,v)$ with the values presented by Kosarim *et al* [26] in Figure 4 of their paper. As can

be seen in [insert Table 3, the present model predicts a slight increase of the cross-sections with the electron impact energy, whereas the model of Kosarim *et al* [26] predicts the opposite. Nevertheless, reasonable agreement is obtained overall between the two models since the ionization cross-sections agree within 80% for v=0, and within 30% for v=20. It should be noted that the model of Kosarim *et al* [26] includes ionization to three states of N_2^+, namely the $X^2\Sigma_g^+$, $A^2\Pi_u$, and $B^2\Sigma_u^+$ states whereas the present model is limited to ionization into states $X^2\Sigma_g^+$ and $A^2\Pi_u$. However, according to Van Zyl and Pendleton [27], the branching ratios of the ionization cross-sections from N_2X to N_2^+X, N_2^+A, and N_2^+B are respectively equal to 0.320±01.47, 0.535±0.112, and 0.145±0.019 for an electron impact energy of 100 eV. Thus, even at these high impact energies, the cross-section for ionization of N_2^+B represents less than 15% of the total ionization cross-section. Therefore, we do not expect ionization from the ground state of N_2 to the B state of N_2^+ to greatly affect the overall ionization.

[insert Table 3]

Predissociation rates

As will be seen in the analysis of the recombination experiments presented in Sections 3 and 4, predissociation plays a key role on the vibrational population distribution of the B state of N_2. Therefore, we describe here the method by which these rates are computed in the CR model.

The predissociation rate constants $\gamma(v,J)$ of the B state of N_2 are taken from Geisen *et al* [24]:

$$\gamma(v,J) = \gamma_1(v) + \gamma_2(v)J(J+1) \tag{5}$$

where the second term on the right hand side of Eqn. (5) is a corrective term corresponding to indirect predissociation of the $^3\Pi_0^f$ component via rotational coupling with the $^3\Pi_1^{ef}$ components (the $^3\Pi_0^f$ component would otherwise remain unpredissociated). This corrective term cannot be larger than the value γ_2^{max} corresponding to the $^3\Pi_1$ predissociation rate constant.

In our CR model, the total predissociation rate constant of a given level v is calculated as a function of T_r by averaging the J-dependent values given by Eqn. (5) as follows:

$$\bar{\gamma}(v) = \frac{1}{Q_{rot}^{N_2(B,v)}(T_r)} \sum_{J \geq J_{\min}} (2J+1)\exp\left(-F_{Bv}(J)/kT_r\right)\gamma(v,J) \tag{6}$$

where J_{min} is the minimum rotational quantum number for which the vibrational level considered predissociates. According to Lofthus and Krupenie [28], these values are J_{min} = 32 for v=12 and J_{min} =0 for v ≥ 13. The summation over J in Eqn. (6) is truncated at the limiting value γ_2^{max}. The values of $\gamma_1(v)$, γ_2 (v), and γ_2^{max} are listed in [insert Table 4. When rate constants for a particular component of a given vibrational level are missing, they are taken as the average rate constants

of that level. The predissociation rate constants of v=12, not given by Geisen *et al*, are assumed to be equal to those of v=13.

[insert Table 4]

In summary, we have presented a vibrationally specific CR model for nitrogen plasmas. This model will be applied later in this paper to the analysis of the recombining nitrogen plasma experiment presented next.

2. Nonequilibrium recombining nitrogen plasma experiment

Experiments were conducted at Stanford University [6] with a recombining atmospheric pressure nitrogen plasma. The experimental set-up is shown in [insert Figure 1. In these experiments, a mixture of ~100 slpm N_2, ~50 slpm argon, and ~2.3 slpm H_2 was inductively heated with a 50 kW RF plasma torch. Argon was added to stabilize the torch operating conditions, and H_2 was added in order to measure the electron number density from the Stark-broadened H_β line. The plasma produced by the torch was accelerated to a velocity of ~1 km/s by passing through a 1 cm diameter torch exit nozzle. From the nozzle, the plasma was then rapidly cooled (within ~250 μs) by flowing through a 15 cm-long water-cooled brass test-section. A shorter test-section, 10 cm in length, was also used to obtain intermediate results at a distance of 10 cm from the nozzle exit. Calorimetric measurements were taken on the water flow used to cool the 10 and 15 cm test-sections. The total heat flux removed by the test-sections was 2.4 and 4.5 kW (±0.1 kW) for the 10- and 15-cm test-sections, respectively.

[insert Figure 1.]

Emission spectroscopy measurements were made using a SPEX model 750M, 0.75-meter, scanning monochromator fitted with a Hamamatsu model R1104 photomultiplier tube. Two 1200 lines/mm gratings blazed at 200 and 500 nm were used to cover the spectral range of the present study. The entrance and exit slits of the monochromator were set to 200 and 400 μm, respectively, yielding a trapezoidal slit function of base 0.66 nm and top 0.22 nm. The spectra measured along the diameter of the plasma at the nozzle and test-section exits were calibrated in absolute intensity using two NIST traceable radiance standards: an Optronics model OL550 standard for wavelengths between 300 and 800 nm and a 1-kW Argon Mini-Arc from Arc Applications Research between 200 and 400 nm.

At the exit of the nozzle (position termed 0 cm), several temperature profiles were obtained by Abel-inverting absolute intensity profiles of various emission lines of N, Ar, and H [6]. As can be seen from Fig. 2a, the good agreement among the various temperature profiles indicates that the plasma is close to LTE at the nozzle exit (which is the inlet of the test-section). The maximum temperature at the centerline is approximately 7200 K. A similar technique was applied at the exit of the 10 cm nozzle (Fig. 2b). At the exit of the 15-cm test-section, a

temperature profile was measured by Abel-inverting lateral profiles of the (0,0) band of the N_2^+ first negative system, as described also in Ref. [6]. The centerline temperature was found to be 4715±100 K (Fig. 2c). Subsequent high-resolution spectroscopy measurements [29] using resolved rotational lines of the N_2^+ first negative system confirmed these measurements with a measured centerline temperature of 4850±100 K.

[insert Figure 2]

At 7200 K, the LTE composition of the plasma is 55% N, 19% N_2, with a balance of argon and hydrogen. The electron mole fraction is 5.5×10^{-4}. At 4715 K, the LTE composition is 63% N_2, 1.3% N, with a balance of argon and hydrogen, and an electron mole fraction of 3.4×10^{-7}. However, because the plasma residence time within the 15-cm test section, 250 μs, is shorter than the characteristic time of atomic nitrogen recombination [30], the atomic nitrogen population tends to freeze and hence is expected to be higher than its LTE value at the exit of the 15-cm test-section.

Electron number densities were also measured using the Stark broadened H_β line at 486 nm, using the technique described in Ref. [31]. The resulting values at 0, 10 and 15 cm are compared in [insert Table 5 with the corresponding LTE number densities at these locations. As can be seen from the table, the electron number density remains close to LTE until at least the exit of the 10 cm test-section. On the other hand, the measured electron number density at 15 cm is about two orders of magnitude larger than the LTE value, consistent with the existence of nonequilibrium conditions at that location.

[insert Table 5]

We now examine the emission spectra at the various locations. Absolute emission spectra between 280 and 800 nm were measured along the plasma diameter, both at the nozzle exit and at the test-section exits. These measured spectra were then compared with LTE spectra calculated with the line-by-line radiation code SPECAIR [31] using the measured gas temperature profiles.

At the nozzle exit, the measured and LTE spectra are in close agreement (see

[insert Figure 3), which supports the existence of LTE conditions at the nozzle exit. At the 10-cm test section exit, the comparison also indicates that the plasma remains close to LTE. At the 15-cm test-section exit, however, the measured spectrum is more intense than the computed LTE spectrum (see [insert Figure 4). In particular, the radiative emission of the first positive system of N_2, second positive system of N_2, and first negative system of N_2^+ is higher than LTE values by factors of about 6, 30, and 10, respectively. These differences indicate that the populations of the emitting vibrational levels are higher than the corresponding LTE values, and thus that these levels follow nonequilibrium distributions. We will now extract the

nonequilibrium vibrational distributions from the measured spectra in order to provide quantitative data to test the CR model.

Note that several bands of NH A-X and OH A-X, the latter coming from some entrainment of ambient air into the plasma plume, were observed in the spectra, and that these bands interfere with the bands of the second positive system of N_2 (C-B transition) and of the first positive system of N_2^+ (B-X). For clarity, we have excluded from [insert Figure 4 the regions where these bands appear, but details of the analysis including these bands are given in Appendix A.

[insert Figure 3]

[insert Figure 4]

The nonequilibrium vibrational population distributions of the observed emitting states at the 15-cm test-section exit were examined. To this end, we multiplied the LTE populations of individual vibrational levels by nonequilibrium factors in SPECAIR, until the predicted spectrum (obtained by solving the radiative transport equation along the plasma diameter) matched the measured spectrum (see Figure 5). Note that this procedure assumes that the nonequilibrium factors are uniform along the plasma diameter. However, because the line-of-sight emission is strongly dominated by the emission from the central region of the plasma, the inferred nonequilibrium factors closely reflect the nonequilibrium population distribution at the center of the plasma. These nonequilibrium factors are defined by:

$$\rho_v = \frac{n_v^{\text{measured}}}{n_v^{\text{LTE}}} \tag{7}$$

where n_v^{measured} and n_v^{LTE} stand respectively for the measured and equilibrium (at the local gas temperature) number density in level v of the B state of N_2. Hence, a nonequilibrium factor greater than unity implies that the vibrational level v is overpopulated with respect to equilibrium at the local gas temperature.

[insert Figure 5]

The measured distribution of nonequilibrium population factors of the N_2 B and C states and of the N_2^+ B state are shown in [insert Figure 6. In this graph, a Boltzmann distribution at T_v= 4715 K would be represented by the straight line ρ_v=1. For the N_2 C and N_2^+ B states, the inferred overpopulation factors do not vary much with the vibrational levels, with values of about 30 for the N_2 C state and 11 for the N_2^+ B state. For the N_2 B state, the measured vibrational distribution is non-Boltzmann, with a marked peak at v=13. We will now compare these measurements with the predictions of the CR model for the B and C states of N_2.

[insert Figure 6]

3. Analysis of the recombining nitrogen experiments

The nitrogen CR model is used in this section to analyze the recombining nitrogen plasma experiments. We are particularly interested in the nonequilibrium vibrational distribution of the B state of N_2, which exhibits a peculiar dependence with a peak at v=13. Argon is not included in the CR model, and we make the assumption that it does not significantly affect the populations of the observed nitrogen states. We therefore consider the case of a pure nitrogen plasma in chemical nonequilibrium. The CR model calculations are performed by making use of the quasi-steady-state (QSS) approximation, which assumes that all excited levels of atoms and molecules are in steady-state, and equations relative to ground levels are replaced with mass conservation equations.

The input parameters of the model are the temperature T = 4715 K, the pressure p = 1 atm, and the number densities of the different species (e, N_2, N_2^+, N, and N^+) at the exit of the 15-cm test-section. The electron number density was measured from the Stark-broadened H_β line and was found to be 7.3×10^{13} cm^{-3}. The N atom overpopulation factor (recall that we expect an overpopulation of nitrogen atoms owing to the finite rate of nitrogen recombination) has been adjusted to $\rho_N = 8.1$ in order to obtain the best possible agreement with the peak of the distribution at v=13. This value will be justified later in Section 4. Thus the N density is set to 1.5×10^{17} cm^{-3}. The density of N_2 is assumed to stay close to its LTE value. Finally, the densities of N^+ and N_2^+ are chosen in such a way that the plasma is electrically neutral and that the charge exchange reaction $N_2 + N^+ \leftrightarrow N_2^+ + N$ is balanced. Note however that the densities of N^+ and N_2^+ have little influence on the N_2 B state population. The final set of input parameters for the CR model computations at 15 cm is summarized in [insert Table 6.

In general, superelastic and electron-electron collisions can have a strong influence on the electron energy distribution function of nitrogen plasmas at low translational temperatures [32, 33]. However, for the conditions of this experiment, the electron density distribution function can be considered to be Maxwellian, as shown by Capitelli *et al* [34]. This observation justifies our assumption in the CR model of a Maxwellian electron energy distribution for the calculation of electron-impact rate coefficients.

[insert Table 6]

The computed vibrational overpopulation factors of the B state of N_2 are plotted in [insert Figure 7 together with the measured overpopulation factors. The curve labeled "CR model" was obtained using the baseline rate coefficients of the CR model. This calculation reproduces the general shape of the experimental curve, with a peak at v = 13, but predicts larger overpopulation

factors at v's above and below 13. Thus we examined the sensitivity of the CR model predictions by varying selected rates.

Curve (a) was calculated by multiplying the N_2 (X-A) and N_2 (X-B) electron-impact excitation and de-excitation rates by a factor of 4, and by dividing the predissociation rate of level N_2 (B,v = 12) by a factor of 5. Note that the value of the N_2 (B,v = 12) predissociation rate used in the baseline CR model is an estimate based on the value measured by Geisen *et al.* [24] for $v = 13$, so that the foregoing adjustment to the rate is reasonable. Similarly, the multiplicative factor of 4 for the X-A and X-B excitation rates is not unreasonable, given the uncertainty on cross-sections for these reactions [35]. With these modified rates, good agreement is obtained with the experimental curve for v=0-13.

Curve (b) presents another calculation in which the rates are modified as in curve (a) and predissociation of levels $v \geq 14$ is neglected. Better agreement with the experimental curve is now obtained for the high-lying levels $v \geq 14$. This result may suggest that the predissociation rates of levels $v \geq 14$ are overestimated in the model, but it may also be due to uncertainties on other rates. The SSH-based VT transfer rate, for instance, may be somewhat inaccurate for the high lying levels, and multi-quantum jumps may have to be considered although typically they should be unimportant at the relatively low temperatures considered here [36, 37]. Nevertheless, these discrepancies are not significant because the experimental uncertainties on overpopulation factors of high-lying levels $v \geq 15$ are quite large (see [insert Figure 6).

[insert Figure 7]

The CR model also predicts the populations of additional vibronic states. [insert Figure 8 shows the vibrational overpopulation factors of the X, A, B, W, B′, and C states of N_2 as a function of the vibrational quantum number v, calculated with the same modified rates as curve (a) of [insert Figure 7. The predicted overpopulation factors for the low-lying levels of all states are in the range 2 to 4. The overpopulation factors of the X, A, and C states increase steadily with v to reach values close to 66, i.e. corresponding to dissociation equilibrium (by this, we mean that the last vibrational level below the dissociation limit of a given electronic state is nearly in equilibrium with the dissociation products). The measured overpopulation factors of the C state of N_2 are practically constant with v, whereas the CR model predicts a sharp increase with v. One possible explanation is that we may overestimate the degree of coupling between the last level (v=4) with nitrogen atoms. In the baseline model, we have simply considered that this level, which is known to be subject to predissociation [28], is fully coupled with the atoms. This assumption appears to be too strong. In addition, it seems important to incorporate in the model the rates of quenching by heavy-particle impact, as well as the rates of V-T and V-V transfer for the C (and B) states of N_2. According to the measurements of Dilecce *et al* [38, 39], these rates are relatively fast and thus could flatten the overpopulation distribution in the C state

of N_2. Finally, the W state overpopulation curve exhibits two inflexion points, and the B′ state overpopulation curve has a local maximum similar to that of the B state. These behaviors are caused by collisional coupling with the predissociating levels of the B state.

[insert Figure 8]

4. Method for measuring N atom densities by emission spectroscopy

Despite the remaining uncertainties on the shape of the vibrational population distribution, the results obtained with the baseline CR model reproduce the observed nonequilibrium distribution of the N_2 B state reasonably well. An interesting result of the analysis presented in the previous section is that vibrational level v=13 of the B state of N_2 appears to be fully coupled with N atoms by predissociation and inverse predissociation. This can be seen by writing the rate equation at steady-state for the population of N_2, B, v=13:

$$\frac{dn_{N_2,B,13}}{dt} = 0 = -n_{N_2,B,13}\left\{k_{\mathrm{v=13}}^{pred} + \sum_{\mathrm{v''}} A_{13\mathrm{v''}} + n_M\left(k_{VT}^{13\to14} + k_{VT}^{13\to12}\right) + n_e k_{ion}^{e} + \sum_{Y=X,A,B',W,C} n_e k_{B,13\to Y}^{e}\right\}$$
$$+ n_N^2 k_{\mathrm{v=13}}^{inv.pr.} + \sum_{\mathrm{Y',v'}} n_{N_2,Y',\mathrm{v'}} A_{\mathrm{v'}13} + n_{N_2,B,14} n_M k_{VT}^{14\to13} + n_{N_2,B,12} n_M k_{VT}^{12\to13} + n_e^2 n_{N_2^+} k_{rec}^{e} + \sum_{Y=X,A,B',W,C} n_Y n_e k_{Y\to B,13}^{e} \quad (8)$$

The numerical values of the depleting terms that appear in the first bracket, as calculated with the CR model, are listed in

[insert Table 7.

[insert Table 7]

It can be seen from

[insert Table 7 that the predissociation term is about 30 times larger than the sum of the other depletion terms. Similarly, it can be shown that the largest term among the processes populating B,v=13 is the inverse predissociation term. It follows that, at steady-state, Eqn. (8) can be approximated by:

$$n_{N_2,B,13} k_{\mathrm{v=13}}^{pred} \approx \left(n_N\right)^2 k_{\mathrm{v=13}}^{inv.pred} \quad (9)$$

Using superscript *eq* to designate equilibrium densities, we also have, from detailed balance, the following relation:

$$n_{N_2,B,13}^{eq} k_{\mathrm{v=13}}^{pred} = \left(n_N^{eq}\right)^2 k_{\mathrm{v=13}}^{inv.pred} \quad (10)$$

Dividing Eqn. (9) by Eqn. (10), we obtain:

$$n_{N_2,B,13} / n_{N_2,B,13}^{eq} \approx \left(n_N / n_N^{eq}\right)^2 \quad (11)$$

which, using nonequilibrium factor notation, can finally be written as:

$$\boxed{\rho_{N_2,B,13} \approx \rho_N^2} \tag{12}$$

Equation (12) expresses a very interesting relation, namely that the overpopulation of the $N_{2,B,v=13}$ state is approximately equal to the square of the overpopulation factor of atomic nitrogen in the ground state. In other words, the vibrational state v=13 is in partial equilibrium with nitrogen atoms in their ground state (in the same way as the last vibrational level in any electronic state tends to be in partial equilibrium with the dissociation products issued from this given state). This relation means that it is possible to use emission spectroscopy to infer ground state atomic nitrogen densities. For our experimental conditions, the overpopulation factor of v=13 is measured to be $\rho_{N2,B,\ v=13} = 66\pm4$. Thus the overpopulation of nitrogen atoms is approximately 8.1±0.3. At 4715±100 K, the equilibrium density of nitrogen atoms in the nitrogen/argon plasma mixture is $1.8\pm0.4\times10^{16}$ cm^{-3}. Multiplying this number by the measured overpopulation factor ρ_N, we infer a nonequilibrium nitrogen atom density of $1.5\pm0.4\times10^{17}$ cm^{-3}, which corresponds to a mole faction of about 10% (whereas the LTE mole fraction of atomic nitrogen at 4715 K is only 1.3%). Note that relation (13) is also valid at pressures lower than one atmosphere because the various depletion terms decrease with decreasing pressure and therefore become even more negligible relative to the rate of predissociation. Thus this technique provides a way to measure absolute densities of ground state nitrogen atoms using emission spectroscopy. It could be particularly useful to determine the density of nitrogen atoms in recombining plasmas such as those produced in arcjets.

Conclusions

Because the characterization of re-entry flow radiation by onboard detectors can only be conveniently performed using optical emission spectroscopy, accurate CR models are needed to infer species densities and temperatures from emission measurements. Collisional-radiative models have recently emerged that can predict certain nonequilibrium plasma conditions reasonably well. In this paper, we described a detailed vibrationally specific CR model and we showed how it can be used to understand and predict the nonequilibrium radiation emitted by a recombining nitrogen plasma at atmospheric pressure. One important result was that the nonequilibrium emission from the N_2 B state can be used to measure the density of ground state atomic nitrogen, hence the dissociation fraction of nitrogen in the flow-field. This method complements existing techniques such as VUV absorption and Two-photon Absorption Laser-Induced Fluorescence (TALIF). In addition, we have provided an experimental test-case with a plasma flow under well-characterized thermodynamic conditions and with detailed quantitative measurements of nonequilibrium vibrational population distributions in the B and C states of N_2 and in the B state of N_2^+. These data can be used to test advanced CR models.

Uncertainties remain on many of the state-specific reaction rates. Accurate cross-sections are needed, in particular for state-specific electron and heavy-particle impact dissociation and excitation rate coefficients. At low pressure, it is also important to take into account possible departures from a Maxwellian distribution for the free electrons. Finally, additional quantitative measurements in nonequilibrium flows are required to further test and validate the nonequilibrium CR models.

Appendix A

In this appendix, details about the fitting of the nonequilibrium spectra at the exit of the 15 cm test-section are presented. The radiative transitions considered in this analysis are the N_2 first (B-A) and second (C-B) positive systems, the N_2^+ first negative system (B-X), the (A-X) transition of OH, and the (A-X) transition of NH. The OH and NH vibrational populations were arbitrarily adjusted to match the features due to these systems in the experimental spectra. Detailed fits over the spectral region 280-470 nm are shown in Figure A.1. The main bands are identified in Table A.1.

[insert Figure A.1]

[insert Table A.1.]

Acknowledgments

Financial support from the US Air Force Office of Scientific Research, NASA Ames Research Center, the European Space Agency, and the French Ministry of Research (Chaire d'Excellence) is gratefully acknowledged.

References

[1] J. Bacri, A. Medani, Physica C, 112 (1982) 101-118.

[2] C. Park, Nonequilibrium Air Radiation (NEQAIR) Program: User's Manual, in, NASA-Ames Research Center, Moffett Field, CA, 1985.

[3] J.P. Sarrette, A.M. Gomes, J. Bacri, C.O. Laux, C.H. Kruger, JQSRT, 53 (1995) 143-152.

[4] J.P. Sarrette, A.M. Gomès, J. Bacri, C.O. Laux, C.H. Kruger, JQSRT, 53 (1995) 125-141.

[5] P. Teulet, S. J.-P., A.-M. Gomès, JQSRT, 70 (2001) 159-187.

[6] R.J. Gessman, C.O. Laux, C.H. Kruger, Experimental study of kinetic mechanisms of recombining atmospheric pressure air plasmas, in: 28th AIAA Plasmadynamics and Lasers Conference, Atlanta, GA, 1997.

[7] M. Cacciatore, M. Capitelli, C. Gorse, Chemical Physics, 66 (1982) 141-151.

[8] G. Colonna, M. Capitelli, D. Giordano, State to State Electron and Vibrational Kinetics in Supersonic Nozzle Expansion: an Improved Model, in: 33rd AIAA Plasmadynamics and Lasers Conference, Maui, HW, 2002.

[9] J. Loureiro, C.M. Ferreira, Journal of Physics D, 22 (1989) 67-75.

[10] L. Pierrot, C.O. Laux, C.H. Kruger, Vibrationally-Specific Collisional-Radiative Model for Nonequilibrium Nitrogen Plasmas, in: 29th AIAA Plasmadynamics and Lasers Conference, Albuquerque, NM, 1998.

[11] L. Pierrot, L. Yu, R.J. Gessman, C.O. Laux, C.H. Kruger, Collisional-radiative modeling of nonequilibrium effects in nitrogen plasmas, in: 30th AIAA Plasmadynamics and Lasers Conference, Norfolk, VA, 1999.

[12] L. Pierrot, Chemical Kinerics and Vibrationally Specific Collisional-Radiative Models for Nonequilibrium Nitrogen Plasmas, in, Stanford University, 1999.

[13] S.M. Chauveau, C.O. Laux, J.D. Kelley, C.H. Kruger, Vibrationally Specific Collisional-Radiative Model for Nonequilibrium Air Plasmas, in: 33rd AIAA Plasmadynamics and Lasers Conference, Maui, HW, 2002.

[14] C. Park, Nonequilibrium Hypersonic Aerothermodynamics, Wiley, New York, 1989.

[15] R.J. Le Roy, Y. Huang, C. Jary, Journal of Chemical Physics, 125 (2006) 164310.

[16] J. Bacri, A. Medani, Physica C, 101 (1980) 399-409.

[17] W. Hwang, Y.-K. Kim, M.E. Rudd, J. Chem. Phys., 104 (1996) 2956-2966.

[18] T. Majeed, D.J. Strickland, J. Phys. Chem. Ref. Data, 26 (1997) 335-349.

[19] J.R. Peterson, A. Le Padellec, H. Danared, G.H. Dunn, M. Larrson, A. Larson, R. Peverall, C.S.R. Stromhlom, M. af Ugglas, W.J. van der Zande, Journal of Chemical Physics, 108 (1998) 1978-1988.

[20] R.F. Stebbings, B.R. Turner, A.C.H. Smith, Journal of Chemical Physics, 38 (1963) 2277.

[21] D.C. Cartwright, S. Trajmar, A. Chutjian, W. Williams, Physical Review A, 16 (1977) 1041-1051.

[22] M.J. Seaton, The Theory of Excitation and Ionization by Electron Impact, in: D.R. Bates (Ed.) Atomic and Molecular Processes, Academic Press, 1962, pp. 375-420.

[23] Y.K. Kazansky, I.S. Yelets, J. Phys. B, 17 (1984) 4767-4783.

[24] H. Geisen, D. Neuschäfer, C. Ottinger, Journal of Chemical Physics, 92 (1990) 104-115.

[25] C.O. Laux, C.H. Kruger, JQSRT, 48 (1992) 9-24.

[26] A.V. Kosarim, B.M. Smirnov, M. Capitelli, R. Celiberto, G. Petrella, A. Laricchiuta, Chemical Physics Letters, 414 (2005) 215-221.

[27] B. Van Zyl, W. Pendleton Jr., Journal of Geophysical Research, 100 (1995) 23755-23762.

[28] A. Lofthus, P.H. Krupenie, J. Phys. Chem. Ref. Data, 6 (1977) 113.

[29] C.O. Laux, R.J. Gessman, C.H. Kruger, F. Roux, F. Michaud, S.P. Davis, JQSRT, 68 (2001) 473-482.

[30] R.J. Gessman, An Experimental Investigation of the Effects of Chemical and Ionizational Nonequilibrium in Recombining Air Plasmas, in: Mechanical Engineering Dept., Stanford University, Stanford, CA, 2000.

[31] C.O. Laux, T.G. Spence, C.H. Kruger, R.N. Zare, Plasma Sources Science and Technology, 12 (2003) 125-138.

[32] C. Gorse, M. Cacciatore, M. Capitelli, S. De Benedictis, G. Dilecce, Chemical Physics, 119 (1988) 63-70.

[33] G. Colonna, C. Gorse, M. Capitelli, R. Winkler, J. Wilhelm, Chemical Physics Letters, 213 (1993) 5-9.

[34] M. Capitelli, S. Longo, N. Dyatko, K. Hassouni, Journal of Thermophysics and Heat Transfer, 12 (1998) 478-481

[35] J. Bacri, A. Medani, Physica C, 101 (1980) 410-419.

[36] F. Esposito, I. Armenise, M. Capitelli, Chemical Physics, 331 (2006) 1-8.

[37] F. Esposito, M. Capitelli, Chemical Physics Letters, 418 (2006) 581-585.

[38] G. Dilecce, P.F. Ambrico, S. De Benedictis, Plasma Sources Science and Technology, 16 (2007) S45-S51.

[39] G. Dilecce, P.F. Ambrico, S. De Benedictis, Chemical Physics Letters, 431 (2006) 241-246.

Table 8. Rovibronic states of N_2 and N_2^+ in the nitrogen CR model. J_{max} is the highest rotational level considered in the ground vibrational level.

N_2			N_2^+		
Electronic state	Vibrational levels	J_{max}	Electronic state	Vibrational levels	J_{max}
$X\ ^1\Sigma_g^+$	0-47	268	$X\ ^2\Sigma_g^+$	0-52	253
$A\ ^3\Sigma_u^+$	0-27	194	$A\ ^2\Pi_u$	0-63	246
$B\ ^3\Pi_g$	0-30	212	$B\ ^2\Sigma_u^+$	0-24	208
$W\ ^3\Delta_u$	0-37	218			
$B'\ ^3\Sigma_u^-$	0-41	225			
$C\ ^3\Pi_u$	0-4	136			

Table 9. Reactions considered in the nitrogen CR model. X stands for the ground electronic state of a given species. Y", Y' refer to any electronic state of molecules. Z", Z' refer to any electronic state of atoms. M stands for any heavy collider (N, N^+, N_2, or N_2^+).

Reaction	Cross-section or rate coefficient data	Remarks
Ionization		
$N(Z")+e \leftrightarrow N^+(X)+e+e$	Drawin [16]	
$N_2(Y",v")+e \leftrightarrow N_2^+(Y',v')+e+e$	BEB [17]	$X\rightarrow X$, $X\rightarrow A$, $A\rightarrow A$, $B\rightarrow X$, $W\rightarrow A$, $B'\rightarrow A$, $C\rightarrow B$
Dissociation		
$N_2(X,v")+e \leftrightarrow N(X)+N(X)+e$	Majeed [18]	Ground state only
$N_2(X,v")+M \leftrightarrow N(X)+N(X)+M$	Park [14]	M=N or N_2
$N_2(Y",v")+M \leftrightarrow N(Z)+N(Z')+M$	V-T and V-V transfer to the last vibrational level below dissociation limit	M=N, N^+, N_2, N_2^+ Y"=A, B, W, B', C
$N_2^+(Y",v")+M \leftrightarrow N(Z)+N^+(X)+M$		M=N, N^+, N_2, N_2^+ Y"=X, A, B
Dissociative recombination		
$N_2^+(X,v")+e \leftrightarrow N(X)+N(X)$	Peterson [19]	Ground state only
Charge exchange		
$N_2(X,v")+N^+(X) \leftrightarrow N_2^+(X,v')+N(X)$	Stebbings [20]	Ground state only
Electronic excitation		
$N(Z")+e \leftrightarrow N(Z')+e$	Park [14]	
$N_2(X,v")+e \leftrightarrow N_2(Y',v')+e$	Cartwright [21]	Y'=A, B, W, B', C
$N_2(Y",v")+e \leftrightarrow N_2(Y',v')+e$	Seaton [22], Drawin [16]	Y, Y'=A, B, W, B', C
$N_2^+(Y",v")+e \leftrightarrow N_2^+(Y',v')+e$	Seaton [22], Drawin [16]	Y, Y'=X, A, B
Vibrational excitation		
$N_2(X,v")+e \leftrightarrow N_2(X,v')+e$	Kazansky [23] (VE)	Ground state only
$N_2(Y",v")+M \leftrightarrow N_2(Y",v"+1)+M$	SSH model (VT)	M=N, N^+, N_2, N_2^+
$N_2^+(Y",v")+M \leftrightarrow N_2^+(Y",v"+1)+M$	SSH model (VT)	M=N, N^+, N_2, N_2^+
$N_2(X,v_1)+N_2(X,v_2) \leftrightarrow N_2(X,v_1-1)+N_2(X,v_2+1)$	SSH model (VV)	Ground state only
$N_2^+(X,v_1)+N_2^+(X,v_2) \leftrightarrow N_2^+(X,v_1-1)+N_2^+(X,v_2+1)$	SSH model (VV)	Ground state only
Predissociation		
$N_2(B,12\leq v\leq 18) \leftrightarrow N(X)+N(X)$	Geisen [24]	
$N_2(C,v=4) \leftrightarrow N(X)+N(X)$		Equilibrium with N(X)
Radiation		
$N(Z') \leftrightarrow N(Z")+h\nu$	Park [14]	
$N_2(Y',v') \leftrightarrow N_2(Y",v")+h\nu$	Laux [25]	
$N_2^+(Y',v') \leftrightarrow N_2^+(Y",v")+h\nu$	Laux [25]	

Table 10. Comparison of vibrationally specific cross-sections for the ionization of levels v=0 and v=20 of the ground state of N_2, as a function of the impacting electron energy, E=20, 30, 50 and 100 eV.

		σ (E=20 eV) $\times 10^{-21}$ m^2	σ (E=30 eV) $\times 10^{-21}$ m^2	σ (E=50 eV) $\times 10^{-21}$ m^2	σ (E=100 eV) $\times 10^{-21}$ m^2
v=0	Present work	3.2	10.9	17.9	20.4
	Kosarim *et al [26]*	1.74	6.1	10.9	
v=20	Present work	3.9	9.3	13.8	15.1
	Kosarim *et al [26]*	2.9	7.5	12.2	

Table 11. Predissociation rate constants for N_2 (B,v) (from Geisen *et al* [24])

v	γ_1 (s^{-1})	γ_2 (s^{-1})	γ_2^{max} (s^{-1})
12	2.6×10^8	1.2×10^5	5.1×10^7
13	2.6×10^8	1.2×10^5	5.1×10^7
14	1.6×10^8	5.4×10^4	2.5×10^7
15	1.1×10^8	3.2×10^4	1.5×10^7
16	2.5×10^7	8.9×10^3	4.3×10^6
17	7×10^6	5.1×10^2	2.5×10^5
18	4×10^6	1.5×10^3	7.5×10^5

Table 12. Measured and equilibrium electron number densities (cm^{-3}) for the N_2/Ar plasma experiments

	0 cm	10 cm	15 cm
Measured	$5.0 \pm 0.3 \times 10^{14}$	$9.8 \pm 1.8 \times 10^{13}$	$7.3 \pm 4.0 \times 10^{13}$
Equilibrium*	$5.4 \pm 0.4 \times 10^{14}$	$6.4 \pm 2.0 \times 10^{13}$	$5.3 \pm 2.7 \times 10^{11}$

*equilibrium is taken at the local gas temperature and 1 atm.

Table 13. Species densities used to simulate the recombining nitrogen plasma conditions at the exit of the 15-cm test-section. T=4715 K, P = 1 atm.

S	n_S^{eq} (cm^{-3})	n_S (cm^{-3})	ρ_S
N	1.8×10^{16}	1.5×10^{17}	8.1
N^+	4.8×10^{10}	3.8×10^{13}	~800
N_2	1.5×10^{18}	1.5×10^{18}	1
N_2^+	3.5×10^{11}	3.5×10^{13}	100
E	4.0×10^{11}	7.3×10^{13}	180

Table 14. Reaction rates (normalized by the population of $n_{N2,B,v=-13}$) for the major depletion processes of N_2 (B,v=13) in the recombining nitrogen plasma (T=4720 K, P=1 atm, ρ_e=180, ρ_N=8.1).

Term from Eqn. (6)	s^{-1}	Process
$k_{v=13}^{pred}$	2.6×10^{8}	Predissociation
$\sum A_{13v''}$	2.0×10^{6}	Radiation
$n_M\left(k_{VT}^{13\to14}+k_{VT}^{13\to12}\right)$	6×10^{6}	Vibrational-translational excitation
$n_e k_{ion}^{e}$	Negligible	Electron impact ionization
$n_e k_{B,13\to X}^{e}$	3.7×10^{4}	Electron impact excitation to X state
$n_e k_{B,13\to A}^{e}$	3.7×10^{5}	Electron impact excitation to A state
$n_e k_{B,13\to W}^{e}$	3.7×10^{6}	Electron impact excitation to W state
$n_e k_{B,13\to B'}^{e}$	3.8×10^{4}	Electron impact excitation to B' state
$n_e k_{B,13\to C}^{e}$	60	Electron impact excitation to C state

Table A.1. Vibrational bands of the N_2 C-B (second positive) and N_2^+ B-X (first negative) systems used to extract the overpopulation factors of the vibrational levels of the N_2 C and N_2^+ B states, as shown in Figures 6a and 6b. These bands can be identified on Figure A.1.

v (emitting level)	Bands of the N_2 C-B system	Bands of the N_2^+ B-X system
0	(0,1) – 357.7 nm (0,2) – 380.4 nm (0,3) – 405.8 nm	(0,0) – 391.1 nm (0,1) – 427.5 nm
1	(1,0) – 315.8 nm (1,3) – 375.4 nm (1,4) – 399.7 nm	(1,0) – 357.9 nm (1,1) – 388.1 nm (1,2) – 423.3 nm
2	(2,0) – 297.5 nm (2,4) – 370.9 nm (2,5) – 394.1 nm	(2,1) – 356.1 nm (2,3) – 419.6 nm
3	(3,1) – 296.1 nm (3,5) – 367,1 nm	(3,2) – 354.6 nm
4	(4,2) – 295.2 nm	

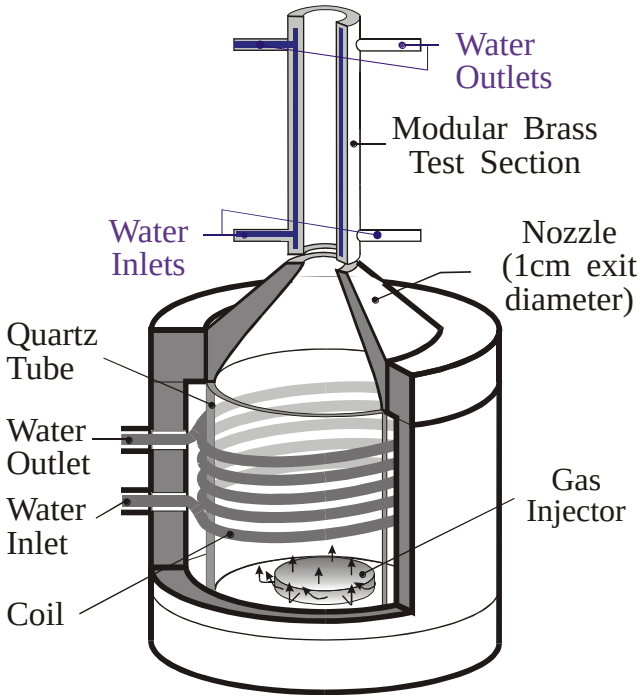

Figure 9. Schematic cross-section of torch head with test-section.

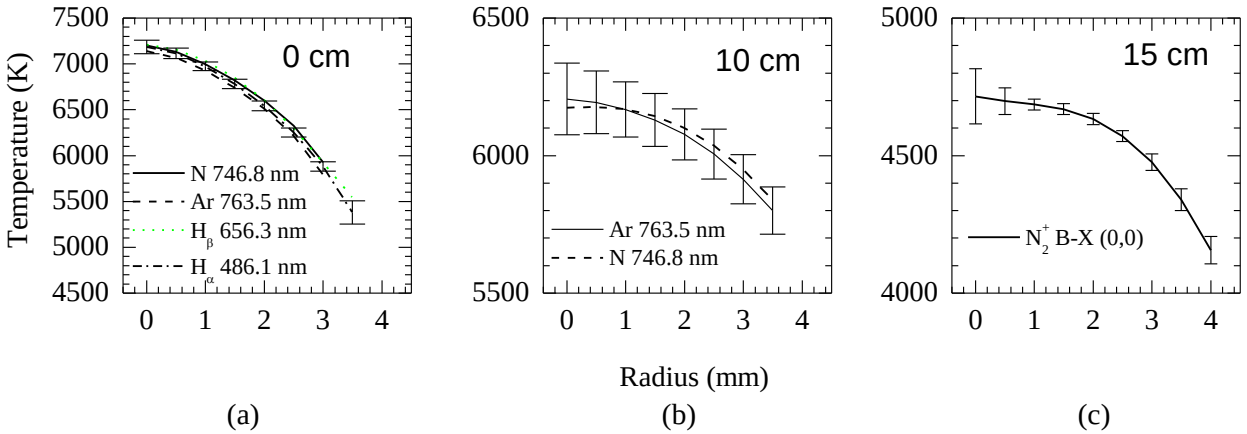

Figure 10. Radial Temperature Profiles of the N_2/Ar Plasma Experiments at nozzle exit (0 cm) and at the exit of the 10 and 15 cm test sections.

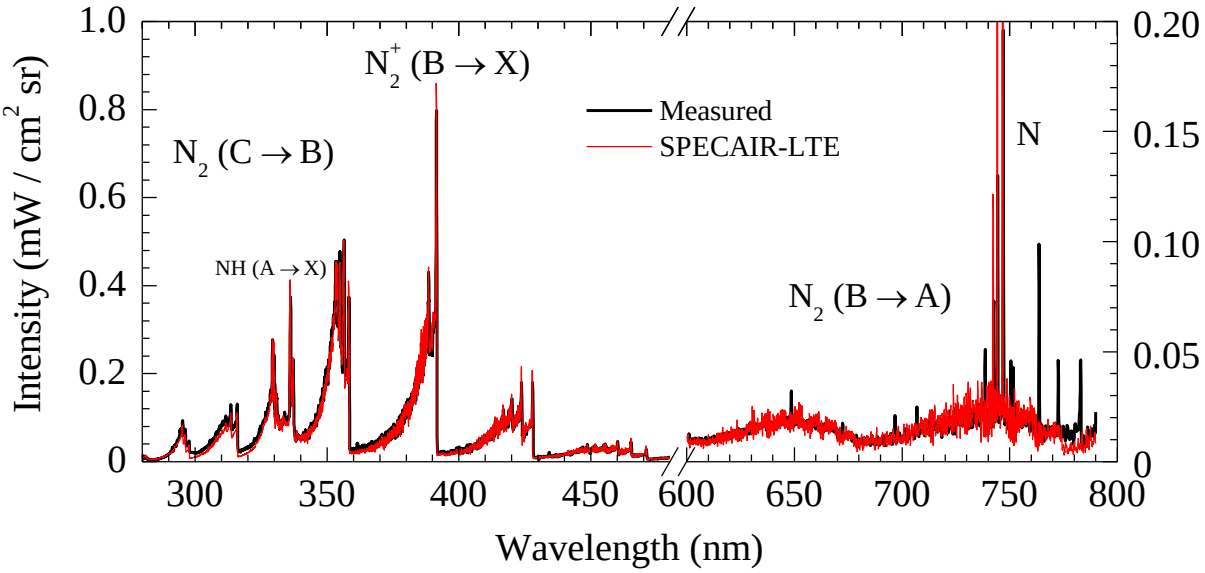

Figure 11. Measured and computed LTE spectra of the nitrogen/argon plasma at the nozzle exit. Several argon lines appear between 650 and 800 nm (not modeled in SPECAIR).

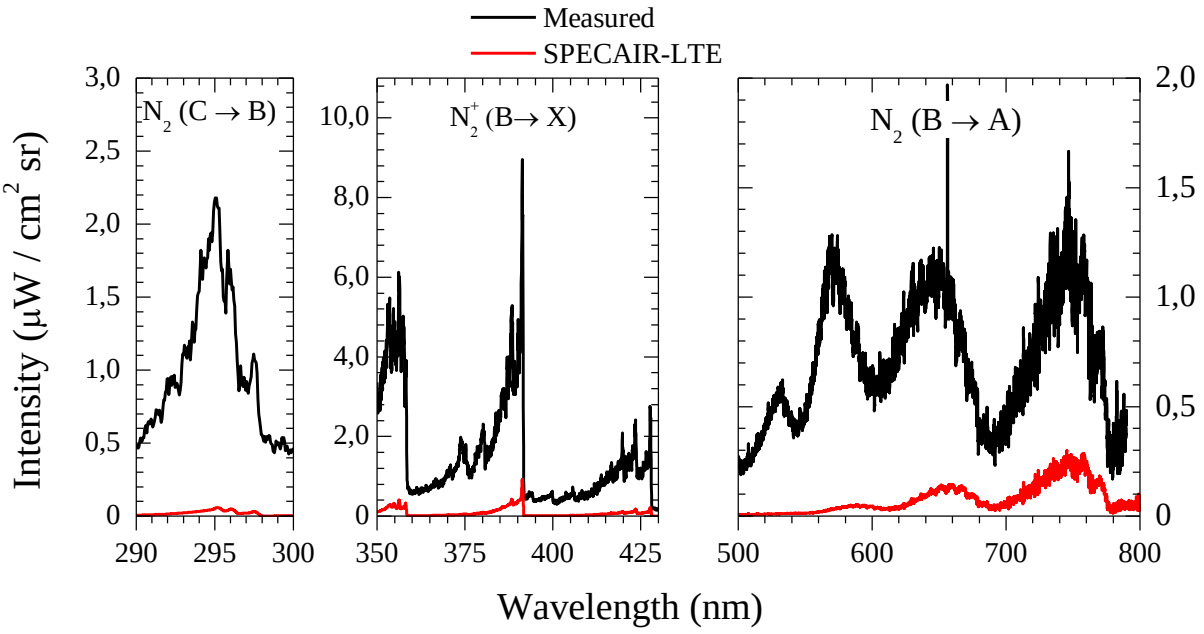

Figure 12. Measured and computed LTE spectra of the nitrogen/argon plasma at the exit of the 15-cm test-section.

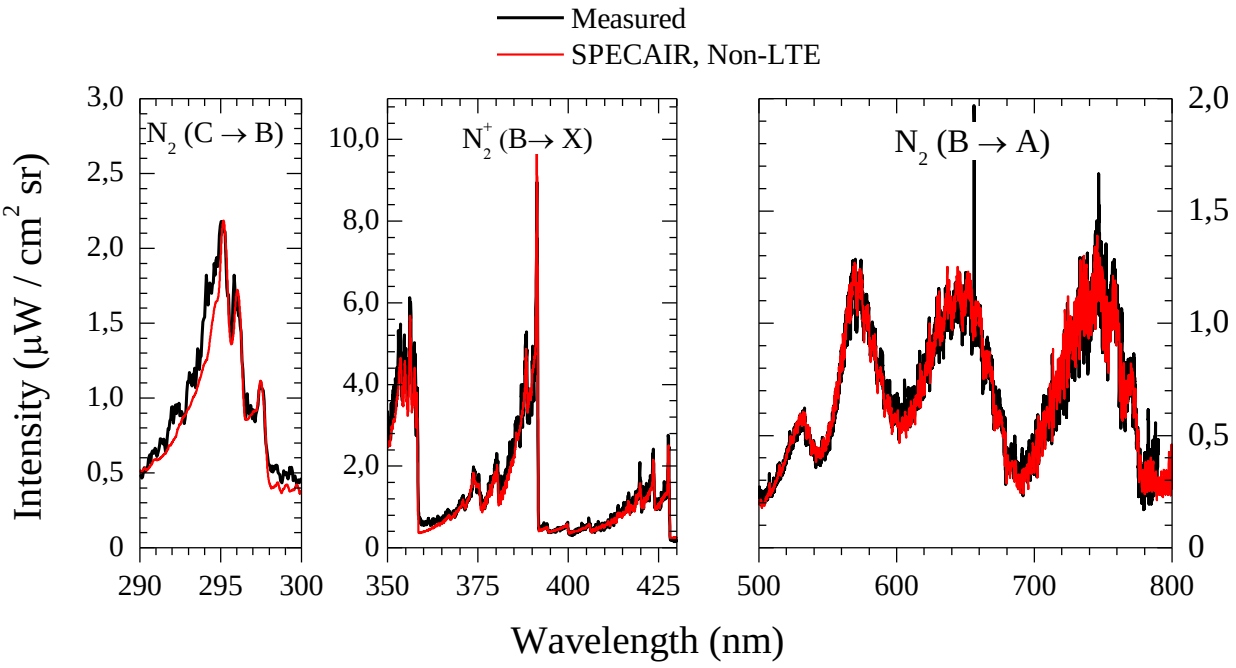

Figure 13. Measured and computed non-LTE (i.e. using the overpopulation factors shown in Figure 6) spectra of the nitrogen/argon plasma at the exit of the 15-cm test-section. Note that the H_α line at 656 nm is not modeled in SPECAIR.

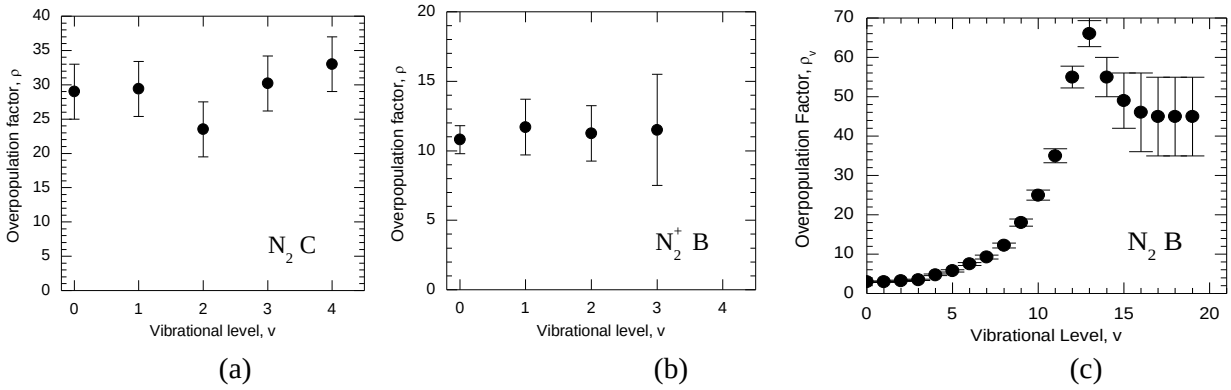

Figure 14. Measured vibrational overpopulation factor distributions in the recombining N_2/Ar plasma. a) N_2 C state, b) N_2^+ B state, c) N_2 B state

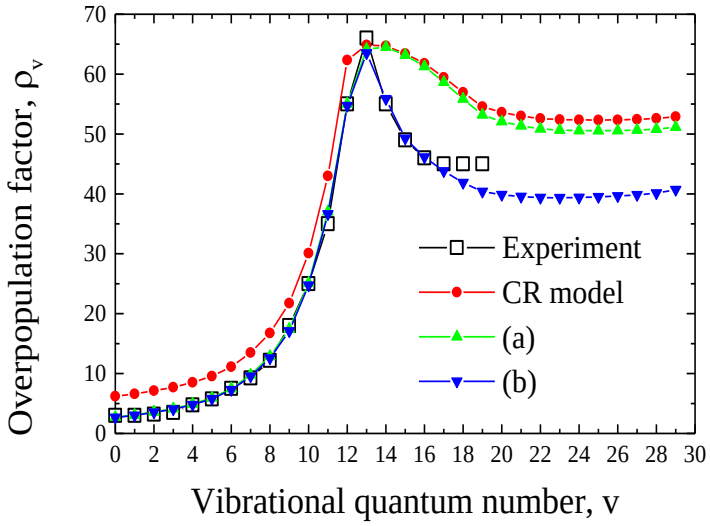

Figure 15. Vibrational overpopulation factors of the N_2 B state. CR model calculation performed with T = 4715 K, p = 1 atm, ρ_e = 180, ρ_N = 8.1. (a): CR model with N_2 (X-A) and N_2 (X-B) electron-impact excitation rates multiplied by 4 and the N_2 (B,v=12) predissociation rate divided by 5. (b): same as (a) without predissociation of levels v≥14 of N_2 (B).

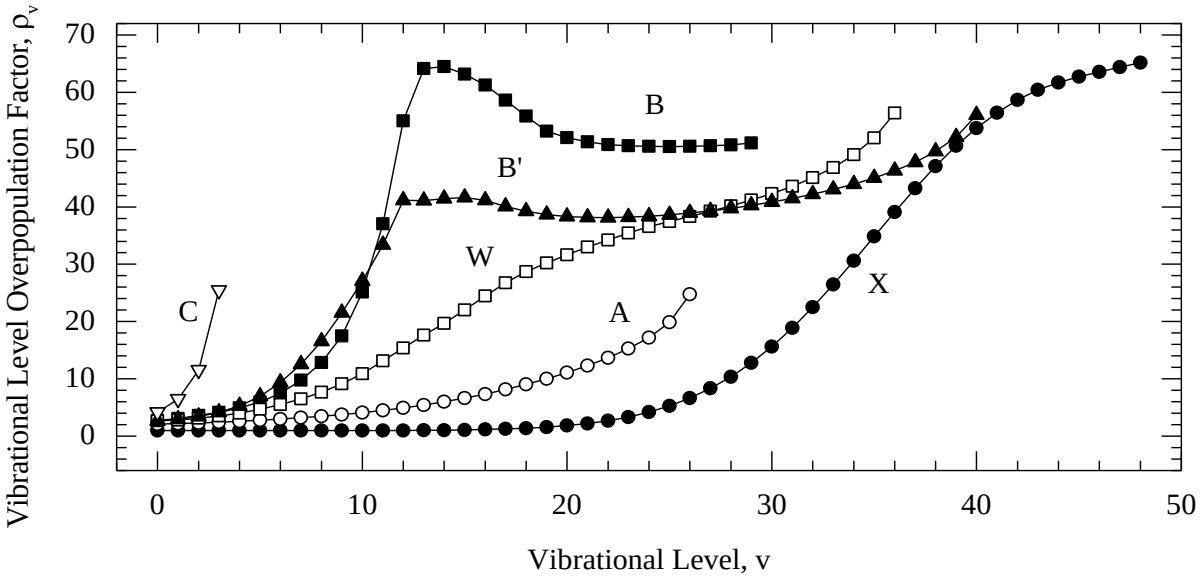

Figure 16. Vibrational overpopulation factors of the X, A, B, W, B′ and C states of N_2. Same conditions as curve (a) of [insert Figure 7.

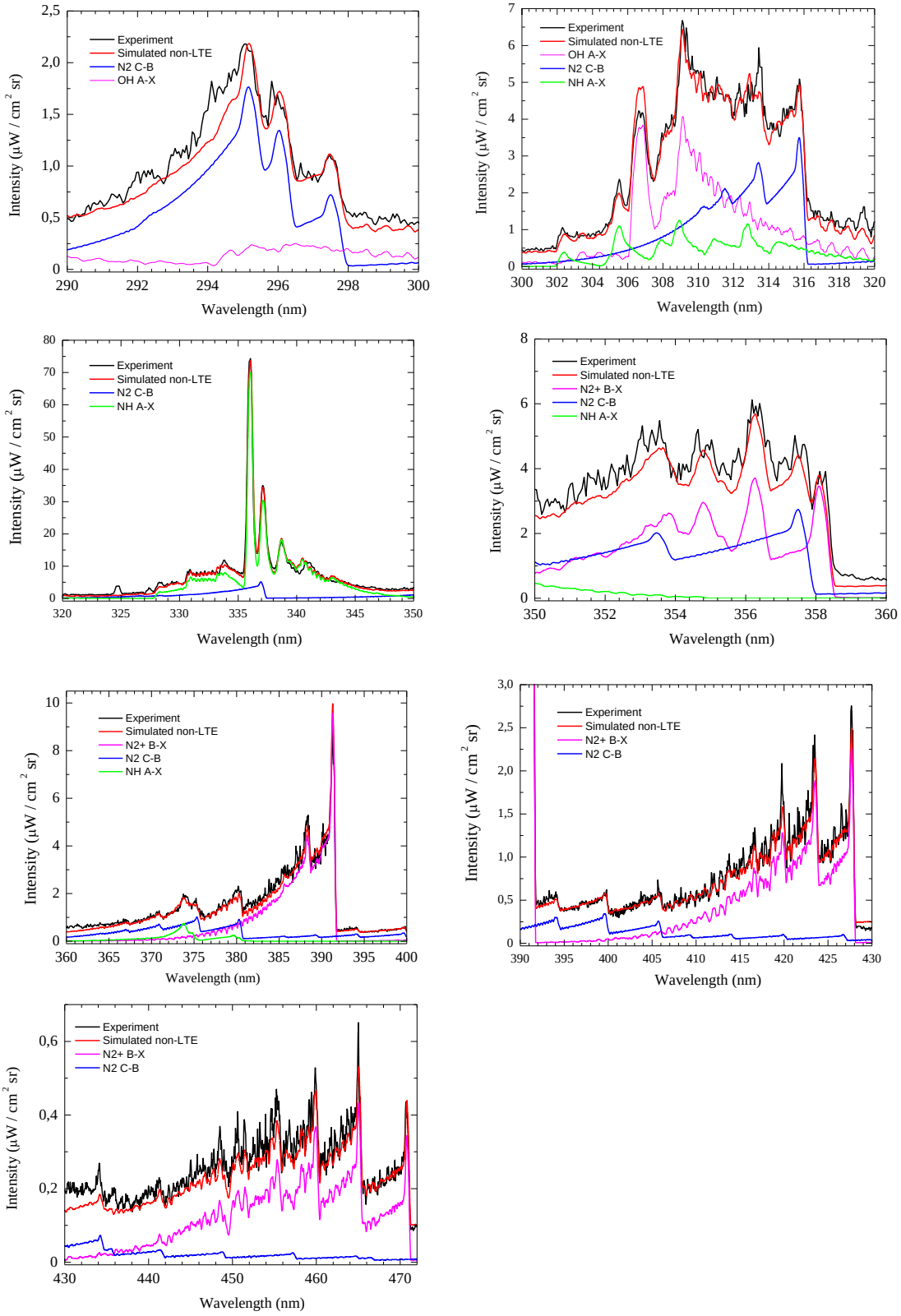

Figure A.1. Details of the spectral fits at the exit of the 15-cm test-section